I.I. ABBASOV,[1] J.I. HUSEYNOV [2]

[1] Azerbaijan State Oil and Industrial University
    (Azerbaijan)
[2] Azerbaijan State Pedagogical University
    (Azerbaijan)

CHARGE-TRANSFER PROCESSES
IN $(SnS)_{1-x}(PrS)_x$ ALLOYS

Interactions in the SnS–PrS alloy system have been studied. On the basis of the results of complex physicochemical analysis, the interval of PrS solubility in SnS is determined. The microrelief of the surface of $Pr_x Sn_{1-x} S$ single crystals is analyzed using a scanning probe microscope operating in the atomic-force regime. The electrical conductivity and the Hall coefficient are researched in a broad temperature interval of 80–800 K. The charge-transfer processes in the objects concerned are analyzed.

K e y w o r d s: solid solutions, chalcogenides, electrical conductivity, donor, Hall coefficient, valence band, light and heavy holes.

1. Introduction

Semiconductor compounds of the $A^{IV}B^{VI}$ type and alloys obtained on their basis are considered to be promising materials for applications in various domains of electronics, or they are already used in infrared radiation sources and detectors, thermoelectric elements, solar batteries, storage elements, and others. The fundamental characteristics of those compounds – such as a narrow energy gap, a high dielectric permittivity, rather a high radiation resistance, and the prevalence of ionic bonds – make the scope of their application even broader [1]. Doping them with impurities that create quasilocal levels also expands the capabilities of their practical application. The corresponding researches are of special importance in fundamental physics as well.

Substances obtained taking advantage of rare-earth metals are widely used for the fabrication of electric energy converters and thermoresistors resistant to radiation, pressure, and moisture. If the $4f$ level in the electron structure of rare-earth metals is filled incompletely, the easy transition $4f - 5d - 6s$ takes place. As a result, the creation of the varying valency by means of mobile electrons at the $4f$ level of those atoms makes the materials obtained with the participation of rare-earth metals to be interesting research objects. From this viewpoint, a capability to produce new promising materials with required physical properties on the basis of alloys and compounds including rare-earth metals makes their research especially challenging [2, 3].

2. Formulation of the Problem.
Objective of Research

Lead chalcogenides (PbX) of the $A^{IV}B^{VI}$ type and solid solutions obtained on their basis with the participation of rare-earth metals are used as materials for the p branch of thermoelectric refrigerators, whereas germanium sulfide (GeS) single crystals with a layered crystal structure are used for holographic inscriptions, in electronic memory units, solar batteries, and so forth [4, 5]. A systematic study of the application potential of various inorganic compounds in photoelectric solar converters showed that many sulfides are characterized by an optical energy gap width that is acceptable for photovoltaic devices [6]. For instance, tin sulfide has the forbidden gap width for direct transitions $E_G^d \approx 1.3$ eV [7], which is close to the optimum theoretical estimate for the effective conversion of solar energy into electric one using unijunction solar cells [8]. By applying SnS as an absorbing layer in photo-electric solar converters, an efficiency of up to 24% can be achieved theoretically [9], which is comparable with the results achieved nowadays with silicon-based and other elements. Among the advantages of SnS, we should also note a low cost of components

required for the preparation of this compound. This fact is associated with a wide spread of tin and sulfur in the Nature, as well as with the non-toxic character of those materials.

The intermediate binary compound SnS with a forbidden gap of 0.95 eV demonstrates both thermoelectric and optical properties. Being characterized by a complicated ion-covalent chemical bonds, it crystallizes into a deformed structure of the NaCl type. One of the main features of SnS is the presence of a certain kind of defects. There are vacancies in both sublattices, and their mutual influence results in the formation of antistructural defects. A high concentration of those defects of about 10^{17} cm^{-3} gives rise to the appearance of the p-conductivity in SnS [9, 10].

The introduction of rare-earth metals into tin monosulfide results in the appearance of a number of physical peculiarities associated with the origin of the defect formation and with the defect interaction. Therefore, the research of the interaction between the SnS and PrS chalcogenides, as well as a comprehensive analysis of charge transport processes in their solid solutions, comprises a scientific and practical interest.

3. Experimental Technique

In this work, using the methods of differential thermal (DTA), microstructural (MSA), and X-ray phase (XPA) analyses, and by measuring the microhardness and density of the SnS–PrS system, the interaction in it is studied, and a part of the state diagram from the SnS side is plotted. In the quasibinary Sn–Pr–S cross-section, in order to determine the interval of the PrS solubility in SnS in $(SnS)_{1-x}(PrS)_x$ compounds, the components were weighed with PrS contents of 0.5, 1, 1.5, 2, 2.5, 3, 3.5, and 4 mol% in accordance with stoichiometry. The alloys were synthesized in a specially selected regime: after 150-h hardening at a temperature of 500 K, the specimens were gradually cooled down to room temperature.

For the determination of melting temperatures in the obtained specimens and the identification of phase transitions in them, the differential thermal analysis (DTA) was carried out on a Perkin Elmer Simultaneous Thermal Analalyzer, STA 6000 (USA). Nitrogen was used as a working gas with a supply rate of 20 ml/s. For the DTA, the examined powder specimen was put into a quartz ampoule. Then air was

pumped out from the ampoule down to a pressure of 10^{-3} Pa. After the sealing, the ampoule was placed in a furnace. The studied specimen was heated at a rate of 5 °C/min up to its melting. Simultaneously, the melting and cooling curves were plotted in a temperature interval from room temperature to 900 °C. The required temperatures were determined from the plots according to the obtained effects.

The phase compositions of the synthesized SnS compound and $(SnS)_{1-x}(PrS)_x$ alloys were determined with the help of microstructural analysis. The researches were carried out on a metallographic microscope MIM-7 at a 200x magnification.

The X-ray diffraction analysis of the alloys of synthesized $Pr_xSn_{1-x}S$ system was performed on a D8 Advance Bruker X-ray diffractometer in the (40 kV, 40 mA) regime, using CuK$_\alpha$ radiation ($\lambda = 1.5406$ Å), and in a TTK 450 K temperature chamber. Diffraction reflections were observed at the displacement angle 2θ within an interval of 0–80°. They were indexed by the TOPAS software. The crystallographic parameters were specified using the EVA software.

The surface relief of $Pr_xSn_{1-x}S$ single crystals characterized by a layered structure was studied by means of a scanning probe microscope operating in the atomic force regime. For obtaining an image, the specimen surface was scanned following a special procedure. When scanning, the probe first moved over the specimen along a definite line. In this case, the magnitude of the signal at the executive element, which was proportional to a surface relief, was registered in a computer memory. Afterward, the probe was returned back to the starting point, passed to the next scanning line, and the process was repeated.

The specific conductance and the Hall coefficient were measured following the standard compensation method in dc electric and electromagnetic fields [11] in a temperature interval of 80–800 K. The experimental errors amounted to 4.2%.

4. Experimental Results

The microimages of those $(SnS)_{1-x}(PrS)_x$ specimens, in which the PrS content was not higher than 3 mol%, clearly demonstrated their homogeneity, which did not differ from that of the SnS microstructure. A second, minor phase was observed, although in a small amount, on the microsections of specimens with PrS

contents of 3.5 and 4 mol%. The study of the micro-hardness dependence on the compound density, which was performed using the radiographic and pycnometric methods, showed that the interval of the PrS solubility in SnS at room temperature is restricted by 3 mol% from above.

Except for the thermal effect corresponding to the melting, no other thermal effects were observed on thermograms obtained for the $Pr_xSn_{1-x}S$ system. The heating-cooling curves demonstrated sharp peaks corresponding to the melting and solidification. Figure 1 exhibits a heating curve for the $Pr_{0.02}Sn_{0.98}S$ specimen. It allows us to assert that congruently melting alloys were formed in the course of this synthesis. In the binary SnS compound, a partial substitution of Sn atoms by Pr ones promotes a decrease of the melting temperature, which testifies that rare-earth metals play the role of softeners in those crystals.

The registered Debye powder patterns and diffraction patterns were identical. The indexing of X-ray patterns showed that, within the solubility interval, the examined SnS-based alloys crystallized in the orthorhombic system. In the solubility interval of the binary SnS compound, since Sn atoms were partially substituted by the atoms of rare-earth metals with a larger radius, the intensity of reflexes decreased, and the parameters of orthorhombic unit cells in the lattice increased additively. In this interval, the lattice parameters grew linearly, and there were no deviations from the Vegard law.

In the X-ray patterns obtained for an interval of 0–3 mol%, no shifts of diffraction lines were observed. Only the variation of their intensity took place, which testified to the formation of an SnS-based solid solutions. The observed growth of lattice parameters, a good agreement of the partial substitution of Sn atoms by Pr ones with a larger radius, and the fulfillment of the Vegard law allow us to say about the formation of substitutional solid solutions on the basis of SnS.

The results of our complex physical and chemical researches show that $Pr_xSn_{1-x}S$ alloys, similarly to the basic SnS substance, crystallize in orthorhombic systems. With increase in the PrS content, a weak growth of the unit cell parameters, density, and microhardness is observed, and the heat effects become shifted toward lower temperatures. For all contents, the density calculated from the X-ray diffraction data
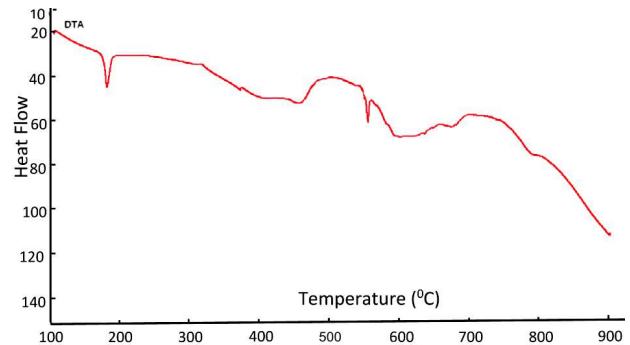

Fig. 1. Heating thermogram for $Pr_{0.02}Sn_{0.98}S$ specimen

is higher than the density determined using the pycnometric method. This fact means that the obtained system of alloys is rich in defects consisting of the vacancies of structural elements.

Figure 2, *a* exhibits a two-dimensional image of a 5×5-μm^2 surface region of a rather homogeneous $Pr_xSn_{1-x}S$ single crystal. The image was obtained with the help of an atomic force microscope. Figure 2, *b* demonstrates a three-dimensional image of a surface section of the same single crystal with a rather homogeneous surface relief. As one can see, the surface of the $Pr_xSn_{1-x}S$ single crystal is quite homogeneous and smooth.

Despite that the SnS single crystals are layered, some roughnesses of the natural cleavage surface can be observed. The histogram analysis of the obtained atomic force microscopy images demonstrates that the natural homogeneity of the SnS single crystal surface changes within the limits of 25 nm. The observation of some roughnesses in the near-surface layer is most likely associated with the presence of weak van der Waals forces between the layers: when the binding forces are destroyed, atomic groups rather than separate atoms remain on the crystal surface [12].

With increase in the rare-earth metal content in the $Pr_xSn_{1-x}S$ single crystals, their surface roughness also grows. In the binary SnS compound, the partial substitution of Sn atoms by rare-earth metal ones with a larger radius results in the enhancement of weak Van der Waals bonds between the layers. Therefore, as the content of Pr in the system of $Pr_xSn_{1-x}S$ alloys increases, the layer-by-layer rejection becomes more complicated, and the roughness of the natural surface grows. The Fourier spectrum obtained using the atomic force microscopy method also confirms this. The surface particles located mainly at the
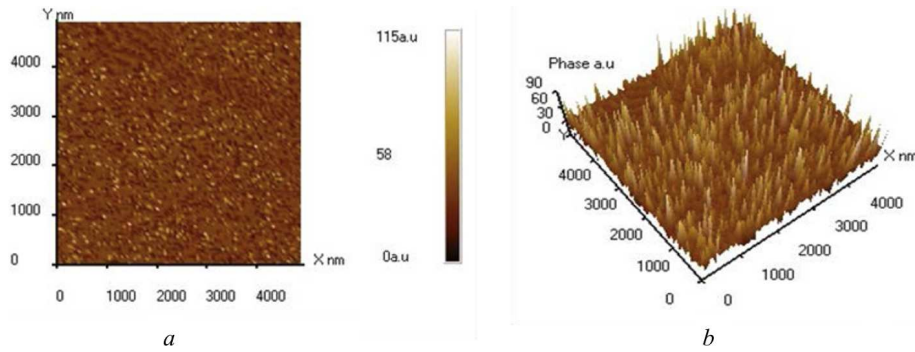
Fig. 2. Two- (*a*) and three-dimensional (*b*) AFM images of the $Pr_xSn_{1-x}S$ single crystal surface

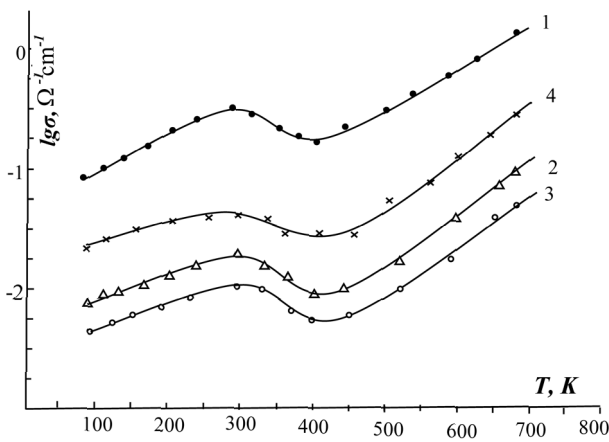**Fig. 3.** Temperature dependences of the specific conductance of $Pr_xSn_{1-x}S$ crystals with $x = 0$ (*1*), 0.005 (*2*), 0.01 (*3*), and 0.02 (*4*)
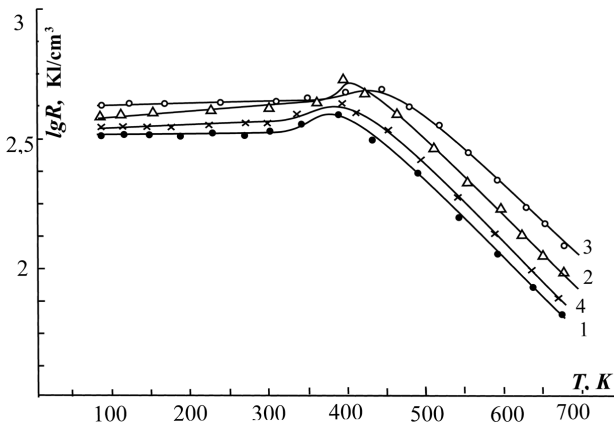

Fig. 4. Temperature dependences of the Hall coefficient of $Pr_xSn_{1-x}S$ crystals with $x = 0$ (*1*), 0.005 (*2*), 0.01 (*3*), and 0.02 (*4*)

center of the spectrum image possess approximately identical dimensions.

With the growth of the Pr content in $Pr_xSn_{1-x}S$ alloys, the specific conductance first decreases and, at $x > 0.01$, increases. At the Pr contents $0 \leq x \leq 0.01$, the occupation of tin vacancies and the change of chalcogenic anti-structural defects result in a reduction of both the charge carrier concentration and the specific conductance. One might say that the further growth of the PrS content does not result in the creation of antistructural defects. It is very probable that the growth of the specific conductance is partially associated with the appearance of charge carriers of the second kind owing to the action of donor Pr atoms.

In Fig. 3, the temperature dependences of the specific conductance of single crystals grown up from the system of $Pr_xSn_{1-x}S$ alloys are shown. As one can see, the specific conductance in the examined crystals has a character inherent in classical semiconductors, if the temperature is varied in an interval of 80–800 K. At low temperatures, the conductivity weakly depends on the temperature. At temperatures $T < 300$ K, the conductivity, being an extrinsic one, is formed as a result of the transition of thermally excited charge carriers from a level localized near the Fermi level onto a delocalized level in the conduction band. With the growth of the Pr content in the alloy, the activation energy of charge carriers decreases.

As the temperature grows from 300 to 500 K, the specific conductance decreases in all researched specimens. In the interval called the impurity depletion region, due to the ionization of all impurities, the concentration of majority charge carriers can be said to remain constant, and their conductivity mainly

886

changes owing to the variation (reduction) of the charge carrier mobility with the temperature.

Above 500 K, the specific conductance drastically grows. The electrons in the valence band, when absorbing the energy equal to or higher than the forbidden gap width, transit into the conduction band and participate in the formation of conductivity. On the basis of the slope of the dependence $\lg \sigma = f\left(\frac{10^3}{T}\right)$ in the high-temperature interval, the temperature dependence of the energy gap width was determined.

If Sn atoms in the SnS crystal lattice are partially substituted by Pr ones, the weak tendency to a reduction of the energy gap width, as the fraction of Pr atoms grows, is observed. This is a result of the ordinary growth of lattice parameters, because Sn atoms with an ionic radius of 0.67 Å are substituted by lanthanide atoms with larger radii (about 1 Å) [16].

The analysis of the temperature dependences of the Hall coefficient for SnS and $(SnS)_{1-x}(PrS)_x$ single crystals demonstrates that, within the temperature interval from the nitrogen temperature to 300 K, i.e. in the extrinsic conductivity region, this parameter remains invariable (Fig. 4). At higher temperatures (300–360 K), the Hall coefficient increases. This anomaly is explained by the presence of traps for electrons in the forbidden band or by the generation of additional acceptors with the temperature growth [14]. As the temperature increases in the intrinsic conductivity interval, the Hall coefficient drastically decreases. A dependence of this type was revealed for the basic SnS compound and its structural analogs. This phenomenon is a result of a complicated character of band structures in those compounds: the valence band consists of two subbands for light and heavy holes, respectively.

In the case of heavy holes, the Hall coefficient is as follows [15]:

$$R = \frac{A}{ec}\frac{p_1\mu_1^2 + p_2\mu_2^2}{(p_1\mu_1 + p_2\mu_2)^2} = R_0 \frac{1 + \frac{p_2}{p_1}b'^2}{\left(1 + \frac{p_2}{p_1}b'\right)^2},$$

where p_1 and p_2 are the concentrations of light and heavy holes, respectively; $b' = \frac{\mu_1}{\mu_2}$ is the ratio between their charges; and $R_0 = \frac{A}{ecp_1}$ is the Hall coefficient at low temperatures. Since b' weakly depends on the temperature, the temperature dependence of the Hall coefficient is governed by the distributions of charge carriers in the valence subbands. Owing to

the low mobility of holes in the second valence band, their contribution to the Hall effect is small. Due to the transition of holes into the second band, their effective concentration decreases, and the Hall coefficient grows.

As one can see from Figs. 3 and 4, the specific conductance of $Pr_xSn_{1-x}S$ single crystals and the temperature behavior of Hall coefficient are identical for all studied crystals. The growth of the Pr content in $Pr_xSn_{1-x}S$ gives rise to an increase of the Hall coefficient or, in other words, to a decrease of the charge carrier concentration. A stable value of the Hall coefficient in a temperature interval of 100–300 K allows those substances to be applied as materials of high quality. Note that the energy gap width determined from the temperature dependence of the Hall coefficient agrees well with the value determined from the specific conductance.

5. Conclusions

The upper limit of the interval of the solubility of PrS in SnS equals 3 mol %. For the Pr contents $0 \leq x \leq 0.01$, the occupation of tin vacancies and the change of chalcogenic antistructural defects result in a reduction of the specific conductance, charge carrier concentration, activation energy, and energy gap width. The temperature dependence of the Hall coefficient is explained well in the framework of the two-band model.

1. D.I. Bletskan. Material synthesis and growth of the single crystals of the type $A^{IV}B^{VI}$ and $A^{IV}B_2^{IV}$. *Chalcogen. Lett.* **4**, 1 (2007).

2. *Physical Properties of Chalcogenides of Rare-Earth Elements,* edited by V.P. Zhuze (Nauka, 1973) (in Russian).

3. E.I. Yarembash, A.A. Eliseev. *Chalcogenides of Rare-Earth Elements* (Nauka, 1975) (in Russian).

4. F.F. Aliev, G.A. Gasanov. Influence of samarium on thermoelectric Q-factor of $Sm_xPb_{1-x}Te$ solid solutions. *Fiz. Tekh. Poluprovodn.* **46**, 313 (2012) (in Russian).

5. P.D. Antunez, J.J. Buckley, R.L Brutchey. Tin and germanium monochalcogenide IV-VI semiconductor nanocrystals for use in solar cells. *Nanoscale* **3**, 2399 (2011).

6. K.N. Reddy, K. Ramesh, R. Ganesan, R.K.T. Reddy, K.R. Gunasekhar, E.S.R. Gopal. Synthesis and characterization of co-evaporated tin sulfide thin films. *Appl. Phys. A* **83**, 133 (2006).

7. A. Luque, A. Marti. *Handbook of Photovoltaic Science and Engineering* (Wiley, 2003).

8. V.F. Gremenok, V.Yu. Rud', Yu.V. Rud', S.A. Bashkirov, V.A. Ivanov. Photosensitive thin-film Schottky barri-

ers In/p-Pb$_x$Sn$_{1-x}$S: creation and properties. *Fiz. Tekh. Poluprovodn.* **45**, 1084 (2011) (in Russian).

9. K.N. Reddy, M. Devika, E.S.R. Gopal. Review on tin (II) sulfide (SnS) material: synthesis, properties, and applications. *Crit. Rev. Solid State Mater. Sci.* **40**, 359 (2015).

10. J. Wang, G. Lian, Z. Xu *et al.* Growth of large-size SnS thin crystals driven by oriented attachment and applications to gas sensors and photodetectors. *ACS Appl. Mater. Interfaces* **8**, 9545 (2016).

11. J.W. Orton, P. Blood. *The Electrical Characterization of Semiconductors: Measurement of Minority Carrier Properties* (Academic Press, 1990).

12. V.L. Mironov. *Fundamentals of Scanning Probe Microscopy* (Tekhnosfera, 2004), p. 197 (in Russian).

13. A.A. Radtsig, B.M. Smirnov. *Reference Data on Atoms, Molecules, and Ions* (Springer, 1986).

14. E.V. Kuchis. *Galvano-Magnetic Effects and Methods of Their Research* (Radio i Svyaz', 1990) (in Russian).

15. R.A. Smith. *Semiconductors* (Cambridge Univ. Press (1978).

16. J.I. Huseynov, M.I. Murguzov, Sh.S. Ismailov. Specific features of self-compensation in Er$_x$Sn$_{1-x}$Se solid solutions. *Fiz. Tekh. Poluprovodn.* **47**, 298 (2013) (in Russian).

I.I. Аббасов, Дж.I. Гусейнов

ПРОЦЕСИ ПЕРЕНЕСЕННЯ ЗАРЯДУ
В СИСТЕМІ СПЛАВІВ (SnS)$_{1-x}$(PrS)$_x$

Р е з ю м е

Досліджено взаємодії в системі SnS–PrS, і за результатами комплексного фізико-хімічного аналізу визначена область розчинності PrS у SnS. За допомогою скануючого зондового мікроскопа в атомно-силовому режимі вивчено мікрорельєф поверхні монокристалів Pr$_x$Sn$_{1-x}$S, досліджені електропровідність σ і коефіцієнт Холла R в широкому інтервалі температур 80–800 K, проаналізовані процеси переносу заряду.